Neutron Compton scattering as a molecular characterization technique: A study on NaHF$_2$

D. Colognesi,[1] A. Pietropaolo,[2] R. Senesi,[2] and A. J. Ramirez-Cuesta[3]

[1]*Istituto dei Sistemi Complessi, Consiglio Nazionale delle Ricerche, Sezione di Firenze, via Madonna del Piano 10, 50019 Sesto Fiorentino, Florence, Italy*

[2]*Dipartimento di Fisica and Centro NAST, Universitá degli Studi di Roma "Tor Vergata," via della Ricerca Scientifica 1, 00133 Rome, Italy*

[3]*ISIS Facility, Rutherford Appleton Laboratory, Chilton, Didcot, Oxon OX11 0QX, United Kingdom*

Inelastic neutron scattering experiments were performed at intermediate and high momentum transfers, up to $85-90$ Å^{-1}, to study the proton momentum distribution in polycrystalline sodium hydrogen fluoride (NaHF$_2$) at low temperature (below 5 K). The H mean kinetic energy was extracted and compared to the results from hydrogen-projected density of phonon states derived from intermediate momentum transfer inelastic neutron scattering and lattice dynamics simulations. A reasonable agreement between the two figures was found. In addition, relevant aspects of high momentum transfer neutron scattering from NaHF$_2$ were explored in detail, ranging from an alternative evaluation of final state effects to the role played by the instrumental resolution and to the possibility to reconstruct the potential felt by a proton from its momentum distribution.

PACS number(s): 34.20.Gj, 61.12.Ex, 63.20.−e

I. INTRODUCTION

Deep inelastic neutron scattering is an experimental technique giving access to information on the atomic momentum distributions in condensed matter. Considering its analogy with the deep inelastic x-ray scattering from core electrons (i.e., the well-known Compton scattering), it is now customary to name the aforementioned neutron technique *neutron Compton scattering* (NCS).[1] The requisites imagined by Gol'danskiĭ for his idea of a "molecular neutronoscopy"[2] are expected to be fulfilled by the NCS technique and therefore one might wonder if NCS has achieved a scientific status similar to that obtained by quasielastic neutron scattering[3] or neutron vibrational spectroscopy.[4] Unfortunately, the answer is not yet fully positive. Just to mention an example, the long-lasting problem of the anomalous deficit of the proton cross sections in various compounds[5] is still an open question, despite several theoretical efforts[6] and experimental tests.[7] The intrinsic interest of the anomalous cross-section deficit and its potentially disruptive effect, which according to some researchers could even shake the theoretical background of the standard neutron scattering theory,[8] are not a main obstacle to the use of NCS as a routine technique in molecular applications. As a matter of fact, a reduction in the intensity of the proton recoil peak is a quantitative phenomenon directly affecting absolute measurements only and is drawn into the domain of standard spectroscopy merely by comparing recoil peaks from different elements or isotopes. In this respect, we have to note that other molecular spectroscopic techniques, such as infrared absorption and Raman scattering, still exhibit a certain difficulty in an accurate prediction of their feature intensities[9] but, nevertheless, are extremely well established and commonly used.

Despite the original application of NCS to superfluid helium and quantum liquids, the technique has now reached a level of detail to tackle studies of molecular systems of increasing complexity. Leaving aside a pioneering NCS experiment on water,[10] this development happened when new powerful spallation neutron sources, such as LANSCE and IPNS in USA, KENS in Japan, and ISIS in UK, became operational during the 1980s.[11] In particular, a permanent NCS instrument, named eVS (electron Volt Spectrometer), was set up at ISIS in 1988 (Ref. 12) and yielded a large number experimental results until 2000, when it was disassembled to be converted into the present epithermal neutron spectrometer VESUVIO.[13] Thus, it was natural, especially at the eVS start, to make heavily use of the advanced theoretical machinery developed by many distinguished scientists[14] to deal with deep inelastic neutron scattering from quantum liquids and anharmonic solids (and even with relativistic electron scattering from nuclear matter). So, concepts like "final state effects," "non-Gaussian momentum distribution," "one-body density matrix," "West scaling" etc., got popular also in connection with a large variety of systems totally remote from the condensed noble gases, ranging from graphite to polymers, molecular hydrogen and deuterium, zirconium hydride, liquid lithium and sodium, ice, and others.[1] Earlier approaches, in spite of being formally rigorous, were quickly found not totally appropriate even in the case of scattering from simple diatomic molecular systems (H$_2$, D$_2$, and N$_2$), and slowly, step by step, some researchers reviewed and updated[15] the theory of deep inelastic neutron scattering from molecules so brilliantly sketched in 1966 by Ivanov and Sayasov,[16] with the only addition of quantized rotations[17] and y scaling (the latter being unknown in the 1960s). A closer look to this molecular approach to NCS, further developed in Refs. 7 and 18 so to cope with molecular crystals and liquids too, showed that it is a simple extension of the model successfully used in vibrational spectroscopy:[4] a sort of harmonic "Meccano/Erector" (i.e., springs and balls), which does not capture the full potential of an ultrafast technique such as NCS and so cannot be considered completely exhaustive. Fortunately, the situation has recently changed. Recent papers have started to consider various exciting aspects of NCS: the anharmonic character of the effective potential felt by protons in some systems,[19] the quantum-indistinguishable character of nuclei on very short time

scales,[20] and the role of the electron dynamics beyond the limit of the Born-Oppenheimer approximation.[21] However, as one can learn from the past, there is a clear need to bridge the gap between NCS experts and the broader community of researchers not directly involved in the development of the deep inelastic neutron scattering theory.

All these considerations prompted the authors of the present paper to elucidate some key concepts in NCS, to present some original views on it, and finally to apply them to a "model compound": sodium hydrogen fluoride ($NaHF_2$). This hydrogen-bonded system is simple enough to allow easy and reliable *ab initio* and semiempirical simulations, but already interesting from the molecular point of view (see below), and to study its NCS spectrum in comparison with the simulation results. The rest of the work will be organized as follows. Section II will be devoted to a quantitative comparison of calculation approaches for the estimate of the so-called final state effects and the effective proton potential reconstruction. Section III will deal with the sample and the experimental procedure of the NCS and vibrational measurements on $NaHF_2$. Data analysis will be sketched in Sec. IV, while Sec. V will report some details about the *ab initio* and semiempirical simulations performed on this system. Finally, Secs. VI and VII will contain the discussion of the results and the conclusions, respectively.

II. FINAL STATE EFFECTS CALCULATION METHODS AND DETERMINATION OF INTERATOMIC POTENTIALS

As we have mentioned in the Introduction, a few aspects of NCS deserve some clarifications, especially in connection with its potential use as a standard molecular spectroscopic technique. In this section, we are going to discuss two points (in Secs. II A and II B) which concern the deep inelastic neutron scattering theory, while a third aspect (on the effect of the energy resolution function) more related to the experimental procedure will be dealt with in Sec. IV.

A. Reaching the impulse approximation and correcting for final state effects

The basic theory of deep inelastic neutron scattering is accurately presented in Ref. 22 and also summarized in Refs. 1 and 14, where the physical rationale of the asymptotic limit in the scattering process (also known as *impulsive approximation*[23]) is shown. The basic tool used in this subject is the usual *self-inelastic structure factor*[24] $S_s(\mathbf{Q},E)$, a function of the energy E and wave-vector transfers $\mathbf{Q}$ from the neutron to the scattering nucleus (having a mass M). After operating the so-called West transform (or y transform) by introducing the scaling variable y and the response function $F(y,\mathbf{Q})$,

$$y = \frac{M}{\hbar^2|\mathbf{Q}|}\left(E - \frac{\hbar^2\mathbf{Q}^2}{2M}\right),$$

$$F(y,\mathbf{Q}) = \frac{\hbar^2|\mathbf{Q}|}{M}S_s(\mathbf{Q},E), \tag{1}$$

one obtains the aforementioned asymptotic limit $J(y,\hat{\mathbf{Q}})$ (with $\hat{\mathbf{Q}}$ being the direction of the wave-vector transfer $\mathbf{Q}$) simply by letting $|\mathbf{Q}|$ go to infinity while keeping y constant:

$$J(y,\hat{\mathbf{Q}}) = \lim_{|\mathbf{Q}|\to\infty;\ y=\text{cost}} F(y,\mathbf{Q}). \tag{2}$$

For scattering nuclei interacting with the rest of the system through a potential without strong short-range repulsion,[25] the asymptotic limit $J(y,\hat{\mathbf{Q}})$ exists and, moreover, is simply related to the single-particle momentum distribution $n(\mathbf{p})$ of the unperturbed system:

$$J(y,\hat{\mathbf{Q}}) = \int d\mathbf{p}\, n(\mathbf{p})\delta(y - \mathbf{p}\cdot\hat{\mathbf{Q}}). \tag{3}$$

It is worth noting that in the rest of the paper, we will not consider the problem of the anomalous cross section and the possible excitation of electronic degrees of freedom via non-Born-Oppenheimer effects. In fact, it is straightforward to verify[21] that the spectral features hypothetically related to the excitation of electronic states would not follow the West scaling. So, assuming, for example, the proton recoil in $NaHF_2$, one could locate the electronic excited part of the spectrum at Δy apart from the standard NCS proton response function, where $\Delta y = 45-90$ Å^{-1}, to be compared with an intrinsic recoil peak width of about 9 Å^{-1} (see below in this section for symbol definitions). This means that the standard NCS proton response would not be marred by electronic excited features, even in the hypothetical case of sizable non-Born-Oppenheimer effects.

Given the experimental impossibility to attain the exact asymptotic limit (i.e., $|\mathbf{Q}|$ and E are always finite), it is a very common question to wonder how far the measurement is from its asymptotic limit. Or in other words, how large one should select $|\mathbf{Q}|$ in order to satisfy Eq. (3) with a given degree of accuracy. Here, the situation starts to become slightly complex, since the exact answer to this problem has been given very generally by Gersch *et al.*[26] through a non-perturbative power series in $|\mathbf{Q}|^{-1}$:

$$F(y,\mathbf{Q}) = J(y,\hat{\mathbf{Q}}) + \sum_{k=1}^{\infty}|\mathbf{Q}|^{-k}F_k(y,\hat{\mathbf{Q}}). \tag{4}$$

Unfortunately, the expressions of the various $F_k(y,\hat{\mathbf{Q}})$ terms [known as *final state effect* (FSE) corrections] are not easy to evaluate. For these reasons, another form of FSE corrections, due to Sears, is generally employed[27] even though its accuracy is sometimes difficult to be rigorously assessed.[28] If the Fourier transform of Eq. (4) is taken, one writes

$$\widetilde{F}(s,\mathbf{Q}) = \widetilde{J}(s,\hat{\mathbf{Q}}) + \sum_{k=1}^{\infty}|\mathbf{Q}|^{-k}\widetilde{F}_k(s,\hat{\mathbf{Q}}), \tag{5}$$

with[26]

$$\tilde{J}(s,\hat{\mathbf{Q}}) = \int d\mathbf{r}\, \rho_1(\mathbf{r}, \mathbf{r} + s\hat{\mathbf{Q}}), \qquad (6)$$

where the formalism of the one-body density matrixes $\rho_1(\mathbf{r},\mathbf{r}+\mathbf{x})$ has been introduced. If a system composed of N nuclei is described by a statistical mixture of many-body wave functions $\Psi_n(\mathbf{r}_1,\ldots,\mathbf{r}_N)$ with statistical weights p_n, and the scattering nucleus is labeled, for example, by i, then the one-body density matrix for the ith nucleus exhibits the following definition:

$$\rho_1^{(i)}(\mathbf{r},\mathbf{r}+\mathbf{x}) = \sum_n p_n \int d\mathbf{r}_1 \cdots \int d\mathbf{r}_N\, \Psi_n^*(\mathbf{r}_1,\ldots,\mathbf{r}_i,\ldots,\mathbf{r}_N)$$
$$\times \Psi_n(\mathbf{r}_1,\ldots,\mathbf{r}_i+\mathbf{x},\ldots,\mathbf{r}_N)\delta(\mathbf{r}-\mathbf{r}_i). \qquad (7)$$

In order to include the FSE corrections $\tilde{F}_k(s,\hat{\mathbf{Q}})$, the potential energy of the system $V(\mathbf{r}_1,\ldots,\mathbf{r}_N)$ has to be specified. In the simple case of an additive pair potential,

$$V(\mathbf{r}_1,\ldots,\mathbf{r}_N) = \sum_{i=1}^{N} \sum_{j<i}^{N} v_{ij}(\mathbf{r}_i,\mathbf{r}_j), \qquad (8)$$

following Ref. 26 $\tilde{F}_1(s,\hat{\mathbf{Q}})$ reads

$$\tilde{F}_1(s,\hat{\mathbf{Q}}) = \frac{iM_i}{\hbar^2}\sum_{i\neq j}^{N} \int d\mathbf{r} \int d\mathbf{x}\, \rho_2^{(i,j)}(\mathbf{r},\mathbf{x};\mathbf{r}+s\hat{\mathbf{Q}},\mathbf{x})$$
$$\times \int_0^s dt[v_{ij}(\mathbf{r}+s\hat{\mathbf{Q}},\mathbf{x}) - v_{ij}(\mathbf{r}+t\hat{\mathbf{Q}},\mathbf{x})], \quad (9)$$

where the semidiagonal two-body density matrix $\rho_2^{(i,j)}$ $\times(\mathbf{r},\mathbf{x};\mathbf{r}+\mathbf{y},\mathbf{x})$ (for the nuclei labeled i and j) has been introduced:

$$\rho_2^{(i,j)}(\mathbf{r},\mathbf{x};\mathbf{r}+\mathbf{y},\mathbf{x})$$
$$= \sum_n p_n \int d\mathbf{r}_1 \cdots \int d\mathbf{r}_N\, \Psi_n^*(\mathbf{r}_1,\ldots,\mathbf{r}_i,\ldots,\mathbf{r}_N)$$
$$\times \Psi_n(\mathbf{r}_1,\ldots,\mathbf{r}_i+\mathbf{y},\ldots,\mathbf{r}_N)\delta(\mathbf{r}-\mathbf{r}_i)\delta(\mathbf{r}-\mathbf{r}_j). \qquad (10)$$

The following FSE correction $\tilde{F}_2(s,\hat{\mathbf{Q}})$ can be found explicitly in Ref. 26 and has been studied in detail in Ref. 29.

At this stage, it is useful to compare Eq. (9) to the corresponding FSE correction (i.e., the term proportional to $|\mathbf{Q}|^{-1}$) suggested by Sears,[27] which in our notation writes

$$\tilde{F}_{1,S}(s,\hat{\mathbf{Q}}) \simeq i\frac{M_i}{2\hbar^2}\sum_{i\neq j}^{N} \left\langle \sum_{\alpha,\beta} \hat{Q}_\alpha \frac{\partial^2 v_{ij}(\mathbf{r}_i,\mathbf{r}_j)}{\partial r_{i,\alpha}\partial r_{j,\beta}} \hat{Q}_\beta \right\rangle \frac{s^3}{6}\tilde{J}(s,\hat{\mathbf{Q}}), \qquad (11)$$

where the quantum average $\langle A(\mathbf{r}_i,\mathbf{r}_j)\rangle$ of a generic position-dependent operator $A(\mathbf{r}_i,\mathbf{r}_j)$ has to be meant as

$$\langle A(\mathbf{r}_i,\mathbf{r}_j)\rangle = \sum_n p_n \int d\mathbf{r}_1 \cdots \int d\mathbf{r}_N\, \Psi_n^*(\mathbf{r}_1,\ldots,\mathbf{r}_N)$$
$$\times A(\mathbf{r}_i,\mathbf{r}_j)\Psi_n(\mathbf{r}_1,\ldots,\mathbf{r}_N)$$
$$= \int d\mathbf{r} \int d\mathbf{x}\, \rho_2^{(i,j)}(\mathbf{r},\mathbf{x};\mathbf{r},\mathbf{x})A(\mathbf{r},\mathbf{x}), \qquad (12)$$

making use of the fully diagonal elements of the two-body density matrix $\rho_2^{(i,j)}(\mathbf{r},\mathbf{x};\mathbf{r},\mathbf{x})$. So, as explained in detail in Ref. 30, Eq. (11) is essentially an approximation of Eq. (9) valid for small values of s. The proof is based on the formula $\rho_2^{(i,j)}(\mathbf{r},\mathbf{x};\mathbf{r}+s\hat{\mathbf{Q}},\mathbf{x}) \approx \rho_2^{(i,j)}(\mathbf{r},\mathbf{x};\mathbf{r},\mathbf{x})\int d\mathbf{r}'\rho_1^{(i)}(\mathbf{r}',\mathbf{r}'+s\hat{\mathbf{Q}})$ in conjunction with a second-order power expansion of integrand containing the potential. An analogous situation is found for the term proportional to $|\mathbf{Q}|^{-2}$ according to Sears:[27]

$$\tilde{F}_{2,S}(s,\hat{\mathbf{Q}}) \simeq \left[\frac{M_i^2}{\hbar^2}\sum_{i\neq j}^{N} \left\langle \left(\sum_\alpha \hat{Q}_\alpha \frac{\partial v_{ij}(\mathbf{r}_i,\mathbf{r}_j)}{\partial r_{i,\alpha}}\right)^2 \right\rangle \frac{s^4}{24} \right.$$
$$\left. + \frac{1}{2}\left(\frac{\tilde{F}_{1,S}(s,\hat{\mathbf{Q}})}{\tilde{J}(s,\hat{\mathbf{Q}})}\right)^2 \right]\tilde{J}(s,\hat{\mathbf{Q}}), \qquad (13)$$

if compared to the $\tilde{F}_2(s,\hat{\mathbf{Q}})$ derived by Gersch et al.[26–28]

A quantitative comparison between the FSE corrections proposed by Gersch et al. and those due to Sears will be presented for $NaHF_2$ in the following sections. In this respect, it is worth mentioning that $\tilde{F}_{1,2,S}(s,\hat{\mathbf{Q}})$ are exact for an ideal harmonic system,[7] and, naturally, $\tilde{F}_{1,2}(s,\hat{\mathbf{Q}})$ and $\tilde{F}_{1,2,S}(s,\hat{\mathbf{Q}})$ coincide. So, discrepancies between the two forms of FSE can be seen as a mark of strongly anharmonic interactions.

B. Single-particle momentum distributions and interatomic potentials

As already reported in the Introduction, one of the most interesting applications of NCS concerns the so-called reconstruction of the Born-Oppenheimer potential felt by protons in condensed matter,[1,19] where a number of highly valuable results have been recently obtained for various systems, ranging from alkali dihydrogen phosphates[19,31] to potassium binoxalate,[32] water and ice (both bulk[33] and confined in carbon nanotubes[34]), acid and base aqueous solutions,[35] etc. Thus, it is important in our view to clarify what kind of "wave function" can be derived from NCS data and, moreover, what kind of "potential" can be reconstructed from these. This clarification is especially important if experimental data have to be compared to *ab initio* or semiempirical simulations, since, as it will be made clear later, very different approximations are implicit in the two data sets. Let us start from the usual many-body Schrödinger equation describing our system composed of N nuclei:

$$-\sum_{j=1}^{N} \frac{\hbar^2}{2M_j}\nabla_j^2\Psi_n(\mathbf{r}_1,\ldots,\mathbf{r}_N) + V(\mathbf{r}_1,\ldots,\mathbf{r}_N)\Psi_n(\mathbf{r}_1,\ldots,\mathbf{r}_N)$$
$$= E_n\Psi_n(\mathbf{r}_1,\ldots,\mathbf{r}_N), \qquad (14)$$

where E_n is the energy eigenvalue corresponding to the sys-

tem eigenstate $\Psi_n(\mathbf{r}_1, \dots, \mathbf{r}_N)$. Taking the Fourier transform of both sides of Eq. (14), representing the transformed functions with a tilde over their symbols, and multiplying the new equation by $\widetilde{\Psi}_n^*(\mathbf{p}_1, \dots, \mathbf{p}_N)$, one can easily write

$$\sum_{j=1}^{N} \frac{\hbar^2 p_j^2}{2M_j} n_n(\mathbf{p}_1, \dots, \mathbf{p}_N)$$

$$+ \int \frac{d\mathbf{q}_1}{(2\pi)^{3/2}} \cdots \int \frac{d\mathbf{q}_N}{(2\pi)^{3/2}} \widetilde{\Psi}_n^*(\mathbf{p}_1, \dots, \mathbf{p}_N) \widetilde{V}(\mathbf{p}_1$$

$$- \mathbf{q}_1, \dots, \mathbf{p}_N - \mathbf{q}_N) \widetilde{\Psi}_n(\mathbf{q}_1, \dots, \mathbf{q}_N) = E_n n_n(\mathbf{p}_1, \dots, \mathbf{p}_N),$$

(15)

where the many-body momentum distribution for the *n*th eigenstate, $n_n(\mathbf{p}_1, \dots, \mathbf{p}_N)$, has been introduced: $n_n(\mathbf{p}_1, \dots, \mathbf{p}_N) = |\widetilde{\Psi}_n(\mathbf{p}_1, \dots, \mathbf{p}_N)|^2$. In the rest of this section, we will focus for sake of simplicity on the ground state *n* = 0, i.e., we will consider our system as kept at zero temperature. It is worth recalling few simple properties of $n_0(\mathbf{p}_1, \dots \dots, \mathbf{p}_N)$:

$$\int d\mathbf{p}_1 \cdots \int d\mathbf{p}_N\, n_0(\mathbf{p}_1, \dots, \mathbf{p}_N) = 1,$$

$$\int d\mathbf{p}_1 \cdots \int d\mathbf{p}_N\, n_0(\mathbf{p}_1, \dots, \mathbf{p}_N)\, \delta(\mathbf{p} - \mathbf{p}_i) = n_0^{(i)}(\mathbf{p}),$$

$$\int d\mathbf{p}_1 \cdots \int d\mathbf{p}_N\, n_0(\mathbf{p}_1, \dots, \mathbf{p}_N) \mathbf{p}_i^2$$

$$= \int d\mathbf{p}_i n_0^{(i)}(\mathbf{p}_i) \mathbf{p}_i^2 = \frac{2M_i}{\hbar^2} \langle E_k \rangle^{(i)}, \qquad (16)$$

where $n_0^{(i)}(\mathbf{p})$ is the single-particle momentum distribution of *i*th nucleus as seen in Eq. (3), and $\langle E_k \rangle^{(i)}$ is its mean kinetic energy. In this way, a link between NCS and Schrödinger equation begins to appear. However, in order to gain a deeper physical sense of our formulas, it is useful to highlight the properties of $R_0(\mathbf{r}_1, \dots, \mathbf{r}_N)$, the multidimensional Fourier transform of $n_0(\mathbf{p}_1, \dots \dots, \mathbf{p}_N)$, related to the system ground state via

$$R_0(\mathbf{r}_1, \dots, \mathbf{r}_N) = \frac{1}{(2\pi)^{3N/2}} \int d\mathbf{x}_1 \cdots \int d\mathbf{x}_N \Psi_0^*(\mathbf{x}_1, \dots, \mathbf{x}_N)$$

$$\times \Psi_0(\mathbf{x}_1 + \mathbf{r}_1, \dots, \mathbf{x}_N + \mathbf{r}_N). \qquad (17)$$

That is to say that $R_0(\mathbf{r}_1, \dots, \mathbf{r}_N)$ is the ground-state autocorrelation function, the analogous of the Patterson function used in x-ray diffraction[36] for describing electron density. The properties sketched in Eq. (16) can now be transferred to the autocorrelation function:

$$(2\pi)^{3N/2} R_0(\mathbf{r}_1 = 0, \dots, \mathbf{r}_N = 0) = 1,$$

$$(2\pi)^{3N/2} R_0(\mathbf{r}_1 = 0, \dots, \mathbf{r}_i = \mathbf{s}, \dots, \mathbf{r}_N = 0)$$

$$= \int d\mathbf{x}_i\, \rho_{1,0}^{(i)}(\mathbf{x}_i, \mathbf{x}_i + \mathbf{s})$$

$$= \int d\mathbf{p}\, e^{i\mathbf{p} \cdot \mathbf{s}} n_0^{(i)}(\mathbf{p}),$$

$$- (2\pi)^{3N/2} \nabla_{\mathbf{s}}^2 R_0(\mathbf{r}_1 = 0, \dots, \mathbf{r}_i = \mathbf{s}, \dots, \mathbf{r}_N = 0) = \frac{2M_i}{\hbar^2} \langle E_k \rangle^{(i)},$$

(18)

where we have also made the link between $R_0(\mathbf{r}_1, \dots, \mathbf{r}_N)$ and the one-body density matrix for the *i*th nucleus in the case of the system ground state [see Eq. (7)] explicit. Now, the Schrödinger equation of Eq. (15) assumes (for the ground state) a third form, which singles out the selected *i*th nucleus, making use of both the autocorrelation function $R_0(\mathbf{r}_1, \dots, \mathbf{r}_N)$ and the wave function $\Psi_n(\mathbf{r}_1, \dots, \mathbf{r}_N)$. Let us put $i = 1$ to simplify the symbolism, but without any loss of generality. One can write

$$\frac{-\hbar^2 \nabla_{\mathbf{s}}^2}{2M_1} R_0(\mathbf{s}, 0, \dots, 0)$$

$$+ \sum_{j=2}^{N} \frac{-\hbar^2 \nabla_j^2}{2M_j} R_0(\mathbf{s}, \mathbf{r}_2, \dots, \mathbf{r}_N) \bigg|_{\mathbf{r}_2 = \cdots = \mathbf{r}_N = 0}$$

$$+ \int \frac{d\mathbf{x}_1}{(2\pi)^{3/2}} \cdots \int \frac{d\mathbf{x}_N}{(2\pi)^{3/2}} \Psi_0^*(\mathbf{x}_1, \mathbf{x}_2, \dots, \mathbf{x}_N)$$

$$\times V(\mathbf{x}_1 + \mathbf{s}, \mathbf{x}_2, \dots, \mathbf{x}_N) \Psi_0(\mathbf{x}_1 + \mathbf{s}, \mathbf{x}_2, \dots, \mathbf{x}_N)$$

$$= E_0 R_0(\mathbf{s}, 0, \dots, 0). \qquad (19)$$

So far, the result is exact. However, if we strive to derive a simple Schrödinger-like single-particle equation concerning the first nucleus with the aim of inverting it, so to "reconstruct" the effective potential felt by this nucleus, we are forced to introduce two rather demanding approximations: (1) the *kinematic* uncorrelation between the first nucleus and all the other nuclei and (2) the "frozen neighbor" (i.e., adiabatic) approximation for the potential generated by spectator nuclei from 2 to *N*.

The first *Ansatz* can be written, for any $j \geq 2$, as

$$\int d\mathbf{p}_2 \cdots \int d\mathbf{p}_N\, n_0(\mathbf{p}_1, \dots, \mathbf{p}_N) \mathbf{p}_j^2 \simeq n_0^{(1)}(\mathbf{p}_1) \frac{2M_j}{\hbar^2} \langle E_k \rangle^{(j)},$$

(20)

or, in the autocorrelation function formalism, as

$$\frac{-\hbar^2}{2M_j} \nabla_j^2 R_0(\mathbf{s}, \mathbf{r}_2, \dots, \mathbf{r}_N) \bigg|_{\mathbf{r}_2 = \cdots = \mathbf{r}_N = 0} \simeq \langle E_k \rangle^{(j)} R_0(\mathbf{s}, 0, \dots, 0). \qquad (21)$$

It expresses the property that $\mathbf{p}_1$ is statistically uncorrelated with all the other $\mathbf{p}_j$. Naturally, in a real molecular system, this statement is, in general, false, since nuclear motions are strongly correlated through precise vibrational normal modes.[4] Nevertheless, it is not impossible to consider that if

the number of normal modes is large and M_1 is quite different from the masses of the neighbor nuclei, then the kinematic approximation becomes a sensible hypothesis surely worth being tested.

The second approximation is conceptually simpler and consists in replacing the potential energy in the integrand in Eq. (19) with its value estimated at appropriate average coordinates $x_2 = \bar{x}_2, \ldots, x_N = \bar{x}_N$ of the spectator nuclei:

$$\int \frac{d\mathbf{x}_2}{(2\pi)^{3/2}} \cdots \int \frac{d\mathbf{x}_N}{(2\pi)^{3/2}} \Psi_0^*(\mathbf{x}_1, \mathbf{x}_2, \ldots, \mathbf{x}_N)$$
$$\times V(\mathbf{x}_1 + \mathbf{s}, \mathbf{x}_2, \ldots, \mathbf{x}_N) \Psi_0(\mathbf{x}_1 + \mathbf{s}, \mathbf{x}_2, \ldots, \mathbf{x}_N)$$
$$\simeq V(\mathbf{x}_1 + \mathbf{s}, \bar{\mathbf{x}}_2, \ldots, \bar{\mathbf{x}}_N) \int \frac{d\mathbf{x}_2}{(2\pi)^{3/2}} \cdots$$
$$\times \int \frac{d\mathbf{x}_N}{(2\pi)^{3/2}} \Psi_0^*(\mathbf{x}_1, \mathbf{x}_2, \ldots, \mathbf{x}_N)$$
$$\times \Psi_0(\mathbf{x}_1 + \mathbf{s}, \mathbf{x}_2, \ldots, \mathbf{x}_N). \quad (22)$$

Clearly, the rationale behind this approximation is that V does not vary too much on the typical lengths of the neighbor nuclei vibrations. In general, this happens, once again, if M_1 is lower than the neighbor nuclei masses. We will study in detail these two *Ansätze* in the case of NaHF$_2$ in the following sections. Plugging Eqs. (21) and (22) into Eq. (19) and exploiting the relationship of Eq. (18), one finally writes an integrodifferential single-particle equation for $\rho_{1,0}^{(1)}(\mathbf{x}_1, \mathbf{x}_1 + \mathbf{s})$:

$$\frac{-\hbar^2}{2M_1} \nabla_{\mathbf{s}}^2 R_0(\mathbf{s}, 0, \ldots, 0) + \frac{1}{(2\pi)^{3N/2}} \int d\mathbf{x}_1$$
$$\times V(\mathbf{x}_1 + \mathbf{s}, \bar{\mathbf{x}}_2, \ldots, \bar{\mathbf{x}}_N) \rho_{1,0}^{(1)}(\mathbf{x}_1, \mathbf{x}_1 + \mathbf{s})$$
$$\simeq \left(E_0 - \sum_{j=2}^{N} \langle E_k \rangle^{(j)} \right) R_0(\mathbf{s}, 0, \ldots, 0), \quad (23)$$

which can also be derived from a fictitious single-particle Schrödinger equation, totally equivalent to Eq. (23):

$$\frac{-\hbar^2}{2M_1} \nabla^2 \varphi_0(\mathbf{r}_1) + V(\mathbf{r}_1, \bar{\mathbf{x}}_2, \ldots, \bar{\mathbf{x}}_N) \varphi_0(\mathbf{r}_1)$$
$$\simeq \left(E_0 - \sum_{j=2}^{N} \langle E_k \rangle^{(j)} \right) \varphi_0(\mathbf{r}_1), \quad (24)$$

assuming the following definition for the pseudo-wave-function of the first nucleus, $\varphi_0(\mathbf{r}_1)$:

$$\rho_{1,0}^{(1)}(\mathbf{x}_1, \mathbf{x}_1 + \mathbf{s}) = \varphi_0^*(\mathbf{x}_1) \varphi_0(\mathbf{x}_1 + \mathbf{s}). \quad (25)$$

Equation (24) can be easily inverted to work out $V(\mathbf{r}_1, \bar{\mathbf{x}}_2, \ldots, \bar{\mathbf{x}}_N)$, the effective potential felt by the first nucleus, once $\varphi_0(\mathbf{r}_1)$ is known from $n_0^{(1)}(\mathbf{p})$ via a simple Fourier transform (if the conditions mentioned in ref. [1] are satisfied):

$$\varphi_0(\mathbf{r}_1) = \frac{1}{(2\pi)^{3/2}} \int d\mathbf{p} \exp(i\mathbf{p} \cdot \mathbf{r}_1) [n_0^{(1)}(\mathbf{p})]^{1/2}. \quad (26)$$

The single-particle momentum distribution can be efficiently obtained from experimental $J(y, \hat{\mathbf{Q}})$ data via the so-called Radon-transform method as suggested by Reiter *et al.*[19] However, it is very important to realize that $\varphi_0(\mathbf{r})$ is by no means the first nucleus wave function which is not defined at all in a system of entangled particles like a molecular solid. It is only a useful mathematical tool to solve Eq. (24), which, in turn, is a rather crude approximation of the true many-body equations reported in various forms in Eqs. (14), (15), and (19). So, the actual physical meaning of the effective potential obtained can be very important but has to be carefully checked considering the two caveats mentioned earlier in this section.

III. SAMPLE DESCRIPTION AND EXPERIMENTAL PROCEDURE

Strong H bonds are probably the most interesting and intriguing category of hydrogen bonds. Recently, H$^+\cdots$N-H ions have been observed in the so-called proton sponges, and there has been even some discussion on the possible role played by strong hydrogen bonds in enzyme catalysis.[37] The prototype of this kind of bonding is surely the hydrogen bifluoride ion [F-H-F]$^-$, one of the first systems to have been intensively studied through x-ray diffraction (1928), infrared spectroscopy (1941), neutron diffraction from an isotopically enriched sample (1952), and NMR (1953). However, for quite a long time, some important aspects of this ion kept their elusive character, such as the supposed centrosymmetric position of the H atom, the exact value of the bond energy, and the extent and nature (i.e., whether mechanical or electrical) of the anharmonicities in the [F-H-F]$^-$ internal vibrations.[38] Nowadays, also with the help of *ab initio* and semiempirical calculations, the large amount of experimental and simulated data has been largely reconciled, obtaining a general consensus on a purely centrosymmetric ionic structure with a H-F distance d_{HF} ranging between d_{HF} =1.132 Å and d_{HF}=1.138 Å and a bond energy of about E_b=163±4 kJ/mole in the gas phase.[39] On the contrary, as far as the study of the ionic vibrations is concerned, no exhaustive and comprehensive representation has been reached, even though some relevant works on Raman,[38,40] IR,[38,40,41] and neutron[40,42,43] spectroscopies have to be mentioned. Especially the last,[43] a high-resolution inelastic neutron scattering measurement on polycrystalline NaHF$_2$ pointed out beyond any doubt the existence of a large LO/TO splitting of ν_2 (bending) but also revealed conspicuous anharmonicity in overtones and combinations. In practice, we have seen that in several cases, hydrogen bifluoride ion has been studied using sodium or potassium as counterions, namely, in NaHF$_2$ or KHF$_2$. These compounds, however, exhibit two entirely different crystal structures at ambient conditions, namely, rhombohedral (R-$3m$, Z'=1)[44] and tetragonal ($I4/mcm$, Z=2),[44] respectively. In addition, two phase transitions have been reported[45] for NaHF$_2$ upon high pressure. The spectroscopic relevance of the existence of these two ambient-condition

TABLE I. Details of the neutron scattering measurements on NaHF$_2$, including spectroscopic technique (NCS stands for neutron Compton scattering, while IINS for incoherent inelastic neutron scattering), label (numbers 1–5 for NCS and letters A and B for IINS), angle φ between the perpendicular to the sample frame and the incident neutron beam, integrated proton current (IPC), and sample temperature T.

Spectroscopic technique	No.	φ (deg)	IPC (μA h)	T (K)
NCS	1	0.0	6327.6	4.49(1)
NCS	2	+45.0	4897.2	4.49(1)
NCS	3	−45.0	4187.9	4.49(1)
NCS	4	+22.5	4493.4	4.49(1)
NCS	5	−22.5	5569.3	4.49(1)
IINS	A	+45.0	1774.4	15.5(9)
IINS	B	−45.0	1535.3	11.5(7)

crystalline structures lies in the number of HF$_2^-$ ions per primitive unit cell: NaHF$_2$ contains just one ion per primitive unit cell. On the contrary, for KHF$_2$, one has always to interact with two crossed ions (moved 3.4 Å apart). For this reason, we have decided that it is largely preferable to make use of sodium bifluoride.

We have performed deep inelastic neutron scattering measurements on a sodium hydrogen fluoride (NaHF$_2$) sample formed by an array of small polycrystalline platelets placed on a thin aluminum frame. Experimental details are summarized in the Table I, where φ represents the angle between the perpendicular to the sample frame and the incident neutron beam, IPC is the integrated proton current, and T is the sample temperature. In the present arrangement, the axis perpendicular to the platelets forms an angle equal to $(45°$-$\varphi)$ with the incident neutron beam (because of "Venetian blind" geometry used to fix the various platelets to the frame). In our measurements, the VESUVIO spectrometer was operated in forward scattering only and was equipped with two sets of Au filters, one cycled in and out of the scattered beams and the other placed in front of four banks of yttrium aluminum perovskite detectors, ranging between $\theta=45.1°$ and $\theta=62.3°$ on both sides of the spectrometer. This method, known as foiling cycling technique,[46] combines the filter difference and resonance detector approaches and can guarantee a reasonable counting rate together with a excellent energy resolution. The raw neutron spectra recorded (see Fig. 1 for an example) clearly exhibit two recoil peaks: a broad and large hump on the left, produced by the hydrogen ions (H$^+$), and a tall and narrow structure determined by all the heavier elements, fluorine (F$^-$), sodium (Na$^+$), and also aluminum (Al), contained in the sample holder frame.

We have also performed *incoherent inelastic neutron scattering* (IINS) measurements on the aforementioned NaHF$_2$ sample (see Table I for experimental details) employing the TOSCA-II vibrational spectrometer.[47] Similarly to the NCS experiment, in the present arrangement, the axis perpendicular to the platelets still formed an angle equal to $(45°-\varphi)$ with the incident neutron beam. The raw neutron scattering
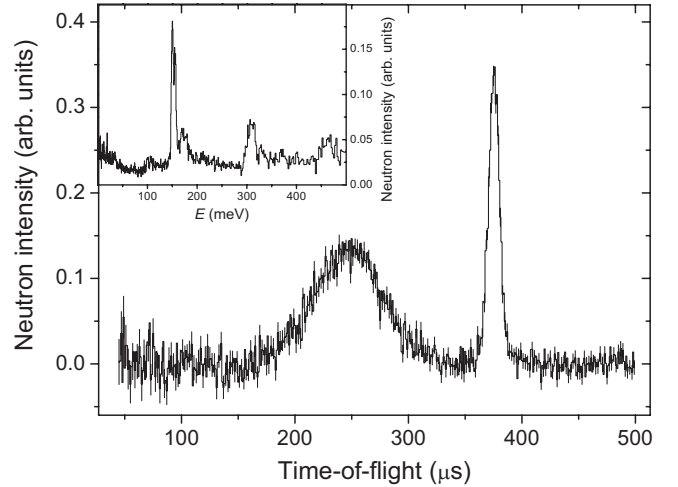
FIG. 1. Main: example of a raw neutron Compton scattering spectrum (time of flight) from NaHF$_2$ recorded on VESUVIO in forward scattering ($\theta=45.1°$) at $T=4.49$ K and $\varphi=0.0°$. Inset: raw neutron scattering spectra from NaHF$_2$ recorded on TOSCA-II in forward scattering at $T=15.5$ K and $\varphi=+45.0°$.

spectra recorded (see inset of Fig. 1) clearly exhibited a low-energy structure (for energies lower than 50 meV) due to a number of NaHF$_2$ lattice modes, then few strong fundamental peaks between 140 and 220 meV, related to the internal vibrations (stretching and bending) of the [FHF]$^-$ ion, and finally a series of overtones and combinations around 300 meV and beyond.

IV. EXPERIMENTAL DATA ANALYSIS

The difference between filter-in and filter-out VESUVIO spectra yielded the experimental NCS time-of-flight profiles. An example of these raw spectra $C(t,\theta)$ for a scattering angle $\theta=45.1°$ is shown in Fig. 1. The spectral contributions given by Na, F, and the aluminum sample holder were carefully subtracted, making use of routines available on the spectrometer[48] and exploiting the wide gap existing, even at the lowest θ values, between the H recoil peak and that related to the heavier nuclei. Multiple scattering contamination was estimated by comparing runs for the same detector (i.e., the same θ) operated at different values of φ to increase the average sample thickness $d(\varphi)$ according to the formula

$$d(\varphi) = \frac{d_0 l_0}{l_0 \left| \cos\left(\frac{\pi}{4}-\varphi\right)\right| + d_0 \left| \sin\left(\frac{\pi}{4}-\varphi\right)\right|}, \quad (27)$$

where d_0 is the actual thickness of the double layer made of the NaHF$_2$ platelets and the aluminum stripe (about 1 mm thick each) and l_0 is the aluminum stripe width (6 mm). Applying Eq. (27), we could characterize the NCS measurements with the following values of average sample thickness: $d(\varphi)=2.1, 2.0, 6.0, 1.9,$ and 2.9 mm for runs 1, 2, 3, 4, and 5, respectively. So, multiple scattering was found to be practically negligible, at least for runs 1, 2, and 4, grouped

together and used in what follows. In particular, for run 2 at $\varphi = +45°$ (i.e., with the aluminum stripes perpendicular to the incoming neutron beam), this finding was confirmed by theoretical calculations which estimated multiple scattering to be only 3.7% of the total scattering in the case of epithermal neutrons. Sample self-shielding was carefully evaluated for all the φ and θ values of the present measurements in the time-of-flight range $50 \ \mu s < t < 500 \ \mu s$ relevant to our experiment. It was found to be essentially flat as a function of t due to the lack of intense neutron absorbing nuclei, and for this reason, no correction was operated on the experimental $C(t, \theta)$.

The experimental time-of-flight spectra, named $C_{H,1}(t, \theta)$ after removing the heavy nuclei signal and checking multiple scattering and self-shielding effects, had to be related to the proton double-differential scattering cross section and, as explained in Sec. II, to the H response functions $F(y, Q)$ (where the dependence on $\hat{Q}$ has been dropped dealing with a polycrystalline sample). A detailed study on the relationship between time-of-flight spectra and response functions has been presented in various works,[7,49] and so here, it is enough to quote the integral formula which links the two physical quantities with each other in the case of the foiling cycling technique:[46]

$$
\begin{aligned}
C_{1,H}(t, \theta) = A \int_{-\infty}^{\infty} d\tau \int_{0}^{\pi} d\vartheta \int_{0}^{\infty} dL_0 \int_{0}^{\infty} dL_1 \, P(\tau, \vartheta, L_0, L_1) \\
\times \int_{0}^{\infty} dE_0 \Phi(E_0) \int_{0}^{\infty} dE_1 \, \eta_\gamma(E_1)[1 - T_{\text{Au}}(E_1)] \\
\times \left(\frac{E_1}{E_0}\right)^{1/2} \frac{F(y, Q)}{Q} \\
\times \delta\left[t - \tau - L_0 \left(\frac{m}{2E_0}\right)^{1/2} - L_1 \left(\frac{m}{2E_1}\right)^{1/2}\right],
\end{aligned} \quad (28)
$$

where A is a constant depending on both the instrument and the sample; τ is the time delay due to the moderator width; ϑ is the actual scattering angle (whose mean value is the nominal scattering angle of the detector considered, θ), $L_{0,1}$ are the initial and final flight paths, respectively; P is the distribution of the four aforementioned random variables; $E_{0,1}$ are the incoming (out-coming) neutron energies; $\Phi(E_0)$ is the incoming neutron flux; $\eta_\gamma(E_1)$ is the gamma production and detection efficiency; and T_{Au} is the transmission of the gold foil cycling in and out of the beam. Needless to say that Q and y are also functions of the actual values of $\{\vartheta, E_0, E_1\}$. However, experimental data are usually transformed into effective $F_{exp}^{(\theta)}(y, Q(y))$ spectra at constant angle via the mean values of $\{\tau, \vartheta, L_0, L_1, E_1\}$, namely, $\{\bar{\tau}, \theta, \overline{L_0}, \overline{L_1}, \overline{E_1}\}$, known from the VESUVIO calibration:[49]

$$
F_{exp}^{(\theta)}(y, Q(y)) = \frac{BM_H}{E_0 \Phi(E_0)} Q C_{1,H}(t, \theta), \quad (29)
$$

where the B is another constant depending on both the instrument and the sample, and M_H is the proton mass. Now, for fixed-angle spectra, y [and then $Q(y)$] are considered as functions of E_0 only, $\{\theta, \overline{E_1}\}$ being fixed parameters, and
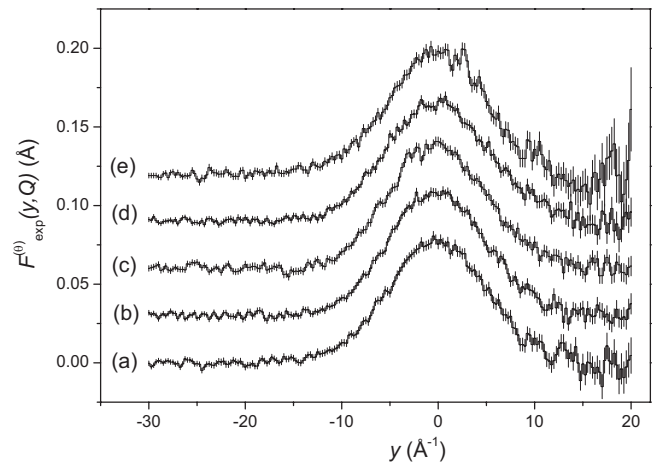
FIG. 2. Examples of the experimentally measured proton response functions in sodium hydrogen fluoride at various scattering angles: (a) +56.4°, (b) +50.4°, (c) +46.63°, (d) −54.9°, and (e) −60.68°. Spectra are vertically shifted for graphic reasons.

through the approximate time-of-flight equation

$$
t \simeq \bar{\tau} + \bar{L}_1 \left(\frac{m}{2\bar{E}_1}\right)^{1/2} + \bar{L}_0 \left(\frac{m}{2E_0}\right)^{1/2}, \quad (30)
$$

y and $Q(y)$ become function of t. Thus, our experimental time-of-flight data were transformed into y-space spectra using a routine available on the spectrometer,[48] and focused to increase the statistical accuracy to obtain fixed-angle data $F_{exp}^{(\theta)}(y, Q(y))$ spanning an interval $\Delta\theta = 0.4°$ of the nominal scattering angle θ (see Fig. 2). These data covered a θ range from 45.2° to 58.0° and from −49.0° to −62.2°. Plugging Eq. (29) into Eq. (28), one can explicitly write the effect of the VESUVIO instrumental resolution on the proton response function to be measured. If the double-differential neutron cross section $\left(\frac{d^2\sigma}{d\Omega dE}\right)$ is introduced,

$$
\left(\frac{d^2\sigma}{d\Omega dE}\right)(E_0, E_1, \vartheta) = \frac{\sigma_H}{4\pi} \left(\frac{E_1}{E_0}\right)^{1/2} \frac{M_H}{\hbar^2 Q} F(y, Q), \quad (31)
$$

then one can write

$$
\begin{aligned}
\left(\frac{d^2\sigma}{d\Omega dE}\right)_{exp} (\epsilon_0, \bar{E}_1, \theta) \\
= D \int_{0}^{\infty} dE_0 \int_{0}^{\infty} dE_1 \int_{-\infty}^{\infty} d\tau \int_{0}^{\pi} d\vartheta \\
\times \int_{0}^{\infty} dL_0 \int_{0}^{\infty} dL_1 P(\tau, \vartheta, L_0, L_1) \frac{\Phi(E_0)}{\Phi(\epsilon_0)} \frac{\eta_\gamma(E_1)}{L_1} \\
\times \left(\frac{E_1}{\epsilon_0}\right)^{3/2} [1 - T_{\text{Au}}(E_1)] \left(\frac{d^2\sigma}{d\Omega dE}\right)(E_0, E_1, \vartheta) \\
\times \delta\left\{E_1 - L_1^2 \left[\frac{\bar{L}_0}{\sqrt{\epsilon_0}} - \frac{L_0}{\sqrt{E_0}} + \frac{\bar{L}_1}{\sqrt{\bar{E}_1}} - (\tau - \bar{\tau})\sqrt{\frac{2}{m}}\right]^{-2}\right\},
\end{aligned}
$$
$$(32)$$

where m is the neutron mass and D is an appropriate instrumental constant. Obviously, given its complexity, Eq. (32) has to be necessarily implemented via a computer code making use of Monte Carlo sampling routines. In the following sections, we will use this scheme to simulate NCS spectra for NaHF$_2$. Due to some numerical difficulties, this method is not widely use in the NCS data analysis. It is generally preferred to relate $F_{exp}^{(\theta)}(y, Q(y))$ to $F(y, Q)$ through a heuristic resolution function $R^{(\theta)}(y)$ (generally, but not always, chosen in a Voigt form):

$$F_{exp}^{(\theta)}(y, Q) \simeq \int dy' \int dQ' F(y', Q') R^{(\theta)}(y - y') \delta(Q(y) - Q'). \tag{33}$$

An assessment about the possible differences between Eqs. (32) and (33) for NaHF$_2$ will be done in Sec. VI.

In the IINS measurements, experimental backscattering and forward-scattering time-of-flight data were transformed into double-differential cross-section spectra, detector by detector, making use of the standard instrumental routines of TOSCA-II,[50] and finally added together in two distinct data blocks. These measurements were corrected for the $(E_1/E_0)^{1/2}$ kinematic factor. At this stage, the important evaluations of self-shielding attenuation and multiple scattering contamination were performed through the analytical approach suggested by Agrawal and Sears in the case of a flat slablike sample.[51] Both procedures were carried out in the framework of the incoherent approximation, totally justified by the preponderance of scattering from the H nuclei and by the polycrystalline nature of the bifluoride sample. Making use of the method explained in Ref. 51 and disregarding the weak inelastic scattering from Al, Na, and F, the input needed for these two corrections was essentially reduced to a rough knowledge of the H-projected density of phonon states, which was approximately set up using the procedure reported in detail in Ref. 52. Multiple scattering contributions were evaluated in the case of $\varphi = +45°$ for the energy transfer interval of interest (i.e., 3 meV $< E <$ 220 meV, the zone of the fundamental bands), amounting on average to 4.8% of the total scattering. However, the multiple scattering component due to two or more inelastic events was found much lower (as expected from Ref. 52) and so was not removed from the spectra. On the contrary, the correction for the sample self-shielding was applied to both backscattering and forward-scattering sets, obtaining the so-called generalized self-inelastic structure factor $\Sigma(Q, E)$.[4] Data from the $\varphi = -45°$ sample arrangement were disregarded because they are too statistically inaccurate and probably plagued with a high level of multiple scattering and self-shielding.

A preliminary extraction of the proton mean kinetic energy from the present NCS data was performed via a simple fitting procedure: the asymptotic $J(y)$ was assumed to have a Gaussian shape and the FSE effects were included following the Sears approach in a simplified form:[48]

$$F(y, Q) \simeq \left[1 - \frac{\sigma^3}{3Q} \frac{d^3}{dy^3} + \frac{\sigma^6}{6Q^2} \frac{d^4}{dy^4} + \frac{1}{2} \left(\frac{\sigma^4}{3Q} \right)^2 \frac{d^6}{dy^6} \right] J(y). \tag{34}$$

Finally, the instrumental resolution was dealt with heuristically as in Eq. (33), making use of Voigt functions whose parameters were estimated through an additional calibration measurement of polycrystalline ZrH$_2$. The result of this fitting procedure (reduced $\chi^2 = 1.27$) was the following estimate of the H mean kinetic energy: $\langle E_k \rangle_H = 111.8 \pm 0.6$ meV.

V. LATTICE DYNAMICAL SIMULATIONS

As already mentioned in the Sec. III, the sodium hydrogen fluoride structure in our experiments is rhombohedral (space group R-$3m$) with one [FHF]$^-$ ion per primitive unit cell. Thus, there are only two lattice parameters (a and c) that have to be specified in order to determine the full crystal structure. *Ab initio* calculations were carried out using plane-wave *density functional theory* (DFT) as implemented by the computer code ABINIT (Ref. 53) in conjunction with the Hartwigsen-Goedecker-Hutter pseudopotentials.[54] As for the type of density functional employed, the *generalized gradient approximation* (GGA) has been preferred using the parametrization introduced by Perdew *et al.*[55] The reasons for this choice can be found in Ref. 56, where it is shown that standard energy minimization methods using GGA give an adequate lattice geometry although the computationally prohibitive thermal and zero-point effects are not included. This choice has also been confirmed by the recent DFT calculations on the same compound performed by Refson *et al.*[57] through the CASTEP code. In addition, the $2s$ and $2p$ semicore electrons for Na were treated as valence states. The convergence achievement was verified with respect to both the number of k points in reciprocal space and the energy cutoff for the plane waves: the present electronic calculation was performed using a mesh of $5 \times 5 \times 5$ points in the k space and a cutoff at 850 eV. In order to calculate a well-defined density of phonon states for NaHF$_2$, phonons were determined on a $16 \times 16 \times 16$ grid of points in the first Brillouin zone. However, a full electronic calculation on such a grid was not necessary since an accurate interpolation procedure through the ANADDB (Ref. 58) program was used. Finally, the actual IINS spectrum was generated using the ACLIMAX code,[59] which takes exactly into accounts thermal and powder-average effects, together with overtones and combinations up to the tenth quantum event. Simulated generalized self-inelastic structure factor $\Sigma(Q, E)$ is reported in Fig. 3 (together with its fundamental component), following the TOSCA-II backscattering kinematic path. As a comparison, the vibrational frequencies obtained for an isolated [FHF]$^-$ ion via DFT[4] are also plotted.

VI. DISCUSSION

The first comparison to be made is between our experimental IINS spectrum and the corresponding DFT simulation. The two curves (both concerning the TOSCA-II backscattering kinematic path) are reported in Fig. 4, together
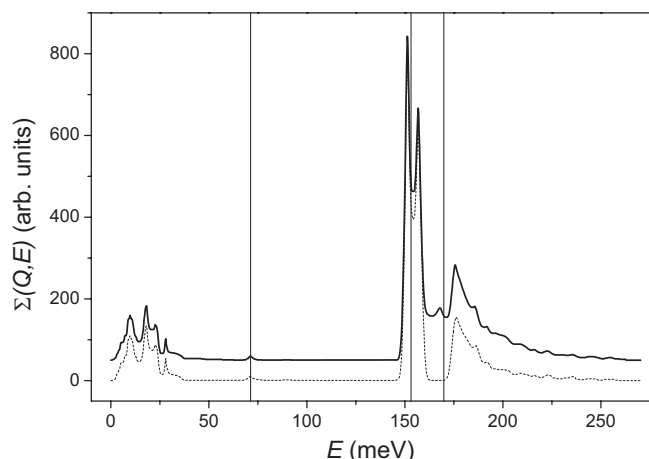
FIG. 3. Simulated generalized incoherent inelastic structure factor $\Sigma(Q,E)$ from the density functional theory calculations. The total $\Sigma(Q,E)$ (full line) and its one-phonon component (dashed line) are reported. The former spectrum is vertically shifted for graphic reasons. Vertical bars represent the simulated vibrational frequencies for an isolated $[FHF]^-$ ion (Ref. 4) Both spectra were evaluated using the backscattering kinematic path.

with a previous IINS measurement[43] obtained from the TFXA spectrometer,[60] the TOSCA predecessor, which exhibited a kinematic path very similar to the TOSCA-II backscattering one. The agreement among the three spectra is very good, especially in the bending region 140 meV $< E$ < 160 meV, where the LO-TO band splitting is clearly visible through the existence of two peaks: at 151 meV and at 156 meV. Further details on this subject can be found in Refs. 4 and 43. The adjacent zone (163 meV $< E$ < 206 meV) is slightly more complex, since, as shown in Fig. 3, it contains two contributions of different nature: the asymmetric stretching mode peaked at 176 meV (fundamen-
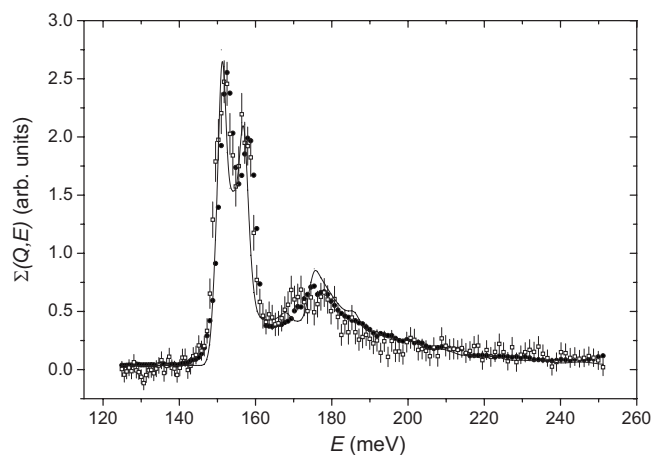
FIG. 4. Comparison among estimates of the generalized incoherent inelastic structure factors $\Sigma(Q,E)$ for NaHF$_2$ derived from the present experiment (empty squares with error bars), a previous neutron scattering measurement (Ref. 43) (black circles), and the present density functional theory calculation (full line). All spectra were calculated using the backscattering kinematic path.

tal) and the combination of the low-energy lattice modes ($E < 37$ meV) with the aforementioned bending ones, lying around 166 meV and partially overlapped with the asymmetric stretching band. In this region, a small disagreement between DFT and IINS is visible due to a slightly different redistribution of the intensities, but this fact does not hamper the overall good quality of the comparison.

After validating the DFT results by means of the IINS measurements, we could exploit the former data to extract an estimate of $\langle E_k \rangle_H$ through the formula

$$\langle E_k \rangle_H = \frac{3}{4} \int_0^\infty G_H(E) E \coth\left(\frac{E}{2k_B T}\right) dE, \quad (35)$$

where $G_H(E)$ is the hydrogen-projected density of phonon states in NaHF$_2$, obtained, in this case, through the simulated phonon frequencies and eigenvectors. From this equation, we worked out the DFT estimate of the proton mean kinetic energy at $T=4$ K, namely, $\langle E_k \rangle_H = 123.6$ meV, which came close to the NCS experimental value, but 9–10 % larger than it. Naturally, one could try to explain this small, but not negligible, discrepancy by various hypothetical reasons (e.g., H vibrational anharmonicity, non-Gaussian hydrogen response function, etc.), but at the present stage, we do not think that these speculations would be solidly justified.

In Sec. II, three relevant problems arise, namely, (1) the more appropriate form for the FSE corrections (i.e., either according to Gersch *et al.* or following Sears) and their mutual relationship, (2) the possibility to reconstruct an effective proton potential in the light of the approximations needed for its extraction, and (3) finally the validity of the convolution approximation expressed in Eq. (33) to deal with the instrumental resolution effects in NCS. We are now in the position to answer these three problems, at least in the case of NaHF$_2$.

A. Evaluation of the final state effects

Dealing with the issue of the final state effects, we immediately face a tremendous task, even for the mere computation of $F_1(y)$: together with a detailed knowledge of the various interatomic potentials $v_{ij}(\mathbf{r}_i, \mathbf{r}_j)$, the evaluation of the semidiagonal two-body density matrixes $\rho_2^{(i,j)}(\mathbf{r}, \mathbf{x}; \mathbf{r}+\mathbf{y}, \mathbf{x})$ is required. For this reason we decided to sketch the following approximate scheme for evaluating $F_1(y)$ and $F_{1,S}(y)$: (a) restraining our description of the FSE to the contribution caused by the interaction between the recoiling proton and the two fluorine nuclei belonging to the same $[FHF]^-$ ion; (b) making use of a semiempirical potential energy function for $[FHF]^-$; (c) evaluating $\rho_2^{(i,j)}(\mathbf{r}, \mathbf{x}; \mathbf{r}+\mathbf{y}, \mathbf{x})$ [including its diagonal elements for computing $F_{1,S}(y)$] through the standard normal mode analysis, which implies the harmonic approximation; and (d) operating a spherical average so to describe a polycrystalline sample.

Points (a) and (c) surely deserve some comments: the decision to limit the FSE calculation to a single $[FHF]^-$ ion might appear as a somehow crude approximation; however, we recall that most of the proton vibrational dynamics is already captured by a simple single-ion description, as

shown in Fig. 3. As a matter of fact, the single-ion model provides in the framework of the harmonic approximation, by the way, a mean kinetic energy value $\langle E_k \rangle_H = 115.9$ meV, not too distant from the experimental and the ABINIT ones. In addition, it is useful to present a heuristic argument based on a fictitious "contact" (i.e., very short ranged, like a billiard ball) interaction to provide a deeper physical understanding of the FSE and the approximations used to evaluate them: let us consider the scaling variable conjugate to y, namely, the proton mean "traveled" distance $s = \hbar Q M_H^{-1} t$. One can immediately compare the effect caused on the hit proton by the presence of a neighbor fluorine nucleus placed at a distance $d_{H\text{-}F} = 1.13$ Å (i.e., belonging to the same bifluoride ion) or at distance $d_{H\cdots F} = 3.82$ Å (i.e., in the nearest bifluoride ion), or even the closest sodium nucleus, $d_{H\cdots Na} = 2.82$ Å.[61] Using the well-known Nyquist-Shannon sampling theorem, we can transform these limiting s values for the proton free recoil into y accuracies ($\Delta y = 2\pi/s$): $\Delta y = 5.56$, 1.64, and 2.23 Å^{-1}, respectively, for H-F, H$\cdots$F, and H$\cdots$Na, to be compared with the typical experimental resolution in the y space, namely, $\Delta y_{res} = 3 - 6$ Å^{-1}. It is evident even from this simple comparison how the role of the intraionic potential is far more relevant than that of the interionic one. As for the use of a harmonically approximate two-body density matrix to compute the FSE, instead of the exact result, it is crucial to stress that this procedure is not at all equivalent to the full harmonic approximation of the FSE. The anharmonic character of the calculation is still contained in the semiempirical potential energy function. On the contrary, if this potential function is also taken as parabolic, then one has the complete harmonic approximation of the FSE, for which, as we have seen, the Sears approach is exact and coincides with that of Gersch *et al.* In addition, since the two-body density matrix is obtained (at zero temperature) only from the vibrational ground state of a [FHF]$^-$ ion, its harmonic approximation appears as thoroughly plausible, since it involves no excited vibrational states, where anharmonicity generally plays a certain role. The anharmonic potential surface describing the [FHF]$^-$ internal dynamics was assumed to be appropriately described by a quartic form by Lohr and Sloboda[62] fitted from their *ab initio* results:

$$V(\mathbf{r}_{F1}, \mathbf{r}_{F2}, \mathbf{r}_H) = \sum_{i=0}^{2} \sum_{j=0}^{2} b_{2i,2j} [(x_{F1} - x_H)^2 + (y_{F1} - y_H)^2]^i$$
$$\times \left[z_H - \frac{1}{2}(z_{F1} + z_{F2}) \right]^{2j}, \quad (36)$$

where z is the molecular axis direction. It is worth noting that the symmetric stretching is not included in this potential surface, which, in fact, has been calculated for a fixed value of the F1-F2 distance (namely $d_{F1\text{-}F2} = 2.292$ Å). However, this lack is totally uninfluential here, since the symmetric stretching does not imply any dynamic displacement of the H nucleus in the [FHF]$^-$ ion. The results of the implementation of Eqs. (9) and (11), respectively, for the Gersch-Rodriguez-Smith and the Sears approaches, have been plotted in Fig. 5, where in panel (A) the aforementioned quantities have been represented in the Fourier-transformed space [i.e., as $\widetilde{F}_1(s)$
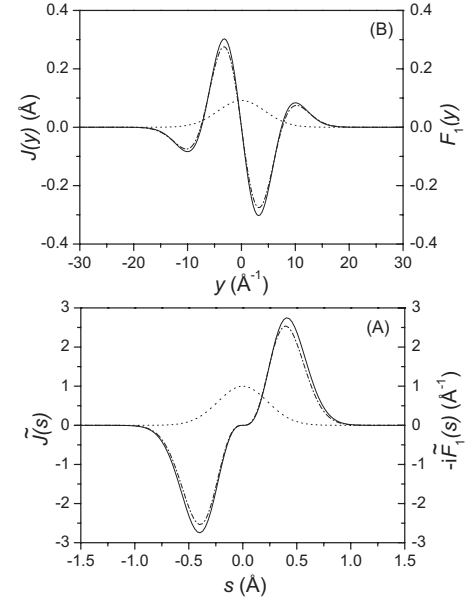
FIG. 5. Estimates of the first term of final state effects, $F_1(y)$, for an [HF$_2$]$^-$ ion through the Gersch-Rodriguez-Smith approach (full line) and the Sears approach (dash-dotted line). The asymptotic limit of the [HF$_2$]$^-$ response function, $J(y)$, is also plotted as a dotted line. In panel (A), the aforementioned quantities are represented in the Fourier-transformed space (i.e., symbols with tilde, functions of the s variable), while in panel (B), the same quantities are plotted in the direct space as functions of the West scaling variable y.

and $\widetilde{F}_{1,S}(s)$], while in panel (B), the same quantities have been plotted in the direct space as $F_1(y)$ and $F_{1,S}(y)$. It is immediately seen that the two approaches do not coincide exactly because of the anharmonic terms in Eq. (36), namely, those for i and/or j larger than 1. However, the observed discrepancies between $F_1(y)$ and $F_{1,S}(y)$ are indeed very modest in the [FHF]$^-$ system and surely below the level of accuracy of the experimentally collected data.

B. Requirements for the extraction of the proton effective potential

In this section, we aim to verify how the two requirements of Sec. II B, namely, the kinematic uncorrelation and the adiabatic approximation, are fulfilled in the case of sodium hydrogen fluoride. Once again, we will approximate this system focusing on a single [FHF]$^-$ ion. In addition, since for both verifications only the vibrational ground state is needed, we will proceed making use of a standard normal mode analysis, which implies the harmonic approximation of the nuclear wave function $\Psi_0(\mathbf{r}_{F1}, \mathbf{r}_{F2}, \mathbf{r}_H)$:

$$\Psi_0(\mathbf{r}_{F1}, \mathbf{r}_{F2}, \mathbf{r}_H) = \psi_0(\mathbf{R}) \prod_{i=1}^{6} \varphi_0^{(i)}(q_i), \quad (37)$$

with $\psi_0(\mathbf{R})$ being the center-of-mass ground-state wave function and $\varphi_0^{(i)}(q_i)$ the ground-state wave function for the ith normal mode q_i, including two librations, two bending

modes, and two stretching modes (symmetric and antisymmetric). So, making use of a reasonable selection of the experimental vibrational frequencies in $NaHF_2$,[4,45,57] it is possible to construct a simple but realistic Gaussian model for $\Psi_0(\mathbf{r}_{F1}, \mathbf{r}_{F2}, \mathbf{r}_H)$, which is needed for testing the adiabatic approximation. As for the momentum distribution $n_0(\mathbf{p}_{F1}, \mathbf{p}_{F2}, \mathbf{p}_H)$, it is possible to prove[17] that Eq. (37) implies the following multiple convolution:

$$
\begin{aligned}
&n_0(\mathbf{p}_{F1}, \mathbf{p}_{F2}, \mathbf{p}_H) \\
&= \int d\mathbf{P} \int d\dot{q}_1 \cdots \int d\dot{q}_6 \, N_0(\mathbf{P}) n_0^{(1)}(\dot{q}_1) \cdots n_0^{(6)} \\
&\quad \times (\dot{q}_6) \delta\left[\mathbf{p}_{F1} - M_F\left(\frac{\mathbf{P}}{M_T} - \hbar^{-1}\sum_{i=1}^{6} \mathbf{C}_{i,F1}\dot{q}_i \right) \right] \\
&\quad \times \delta\left[\mathbf{p}_{F2} - M_F\left(\frac{\mathbf{P}}{M_T} - \hbar^{-1}\sum_{j=1}^{6} \mathbf{C}_{j,F2}\dot{q}_j \right) \right] \\
&\quad \times \delta\left[\mathbf{p}_H - M_H\left(\frac{\mathbf{P}}{M_T} - \hbar^{-1}\sum_{k=1}^{6} \mathbf{C}_{k,H}\dot{q}_k \right) \right],
\end{aligned}
\tag{38}
$$

with $N_0(\mathbf{P})$ being the center-of-mass ground-state momentum distribution, $n_0^{(i)}(\dot{q}_i)$ the ith normal mode ground-state momentum distribution, $\mathbf{C}_{j,n}$ the polarization vector relating the jth normal mode to the nth nucleus, and M_T the total ionic mass. It is worth recalling that $\dot{q}_i$ is the conjugate momentum of the ith normal mode, which (in the coordinate representation) corresponds to the differential operator $-i\hbar\frac{\partial}{\partial q_i}$. Exploiting the properties of the multivariate Gaussian distribution, Eq. (38) simply reads

$$
n_0(\mathbf{p}_{F1}, \mathbf{p}_{F2}, \mathbf{p}_H) = \frac{1}{(2\pi)^{9/2} \det V_{n,m}} \exp\left(-\frac{1}{2}\sum_{n,m}^{9} p_n V_{n,m}^{-1} p_m \right),
\tag{39}
$$

where the simple convention $(p_1, p_2, \ldots, p_9) = (\mathbf{p}_{F1}, \mathbf{p}_H, \mathbf{p}_F)$ is used and the covariance matrix $V_{n,m}$ is approximated (in the $T=0$ limit), after spherically averaging the small center-of-mass contribution, by

$$
\begin{aligned}
\hbar^2 V_{n,m} \simeq &\frac{2M_n M_m}{3M_T}\langle E_k \rangle_{CoM}[\delta_{n,m} + \delta_{l(n),m} + \delta_{k(n),m}] \\
&+ M_n M_m \sum_{i=1}^{6} C_{i,n}^* C_{i,m} \frac{\hbar\omega_i}{2},
\end{aligned}
\tag{40}
$$

where $\langle E_k \rangle_{CoM}$ is the center-of-mass mean kinetic energy, $l(n) = [(n+2)\bmod 9]+1$, $k(n) = [(n+5)\bmod 9]+1$, and the same convention as above, namely, $(C_{i,1}, C_{i,2}, \ldots, C_{i,9}) = (\mathbf{C}_{i,F1}, \mathbf{C}_{i,H}, \mathbf{C}_{i,F2})$ and $(M_1, M_2, M_3, M_4, \ldots, M_9) = (M_F, M_F, M_F, M_H, \ldots, M_F)$, applies. As for the frozen neighbor (adiabatic) approximation, we have calculated, via Eqs. (36) and (37), the following effective potential $W(\mathbf{s})$, a physical quantity sensitive to this approximation in the light of Eq. (22). Once the calculation was operated exactly,

$$
W(\mathbf{s}) = \frac{\int d\mathbf{r}_H \int d\mathbf{r}_{F1} \int d\mathbf{r}_{F2} \Psi_0^*(\mathbf{r}_{F1}, \mathbf{r}_H, \mathbf{r}_{F2}) V(\mathbf{r}_{F1}, \mathbf{r}_H + \mathbf{s}, \mathbf{r}_{F2}) \Psi_0(\mathbf{r}_{F1}, \mathbf{r}_H + \mathbf{s}, \mathbf{r}_{F2})}{\int d\mathbf{r}_H \int d\mathbf{r}_{F1} \int d\mathbf{r}_{F2} \Psi_0^*(\mathbf{r}_{F1}, \mathbf{r}_H, \mathbf{r}_{F2}) \Psi_0(\mathbf{r}_{F1}, \mathbf{r}_H + \mathbf{s}, \mathbf{r}_{F2})},
\tag{41}
$$

and later implementing the adiabatic scheme,

$$
W(\mathbf{s}) \simeq \frac{\int d\mathbf{r}_H V(\bar{\mathbf{r}}_{F1}, \mathbf{r}_H + \mathbf{s}, \bar{\mathbf{r}}_{F2}) \int d\mathbf{r}_{F1} \int d\mathbf{r}_{F2} \Psi_0^*(\mathbf{r}_{F1}, \mathbf{r}_H, \mathbf{r}_{F2}) \Psi_0(\mathbf{r}_{F1}, \mathbf{r}_H + \mathbf{s}, \mathbf{r}_{F2})}{\int d\mathbf{r}_H \int d\mathbf{r}_{F1} \int d\mathbf{r}_{F2} \Psi_0^*(\mathbf{r}_{F1}, \mathbf{r}_H, \mathbf{r}_{F2}) \Psi_0(\mathbf{r}_{F1}, \mathbf{r}_H + \mathbf{s}, \mathbf{r}_{F2})},
\tag{42}
$$

where $\bar{r}_{F1}$ and $\bar{r}_{F2}$ are the fluorine atom equilibrium positions. Numerical results are reported in Fig. 6 as a function of $|\mathbf{s}|$ for selected values of θ, the angle between the vector $\mathbf{s}$ and the line joining the two F atoms. It is immediately evident that in our system, the mentioned frozen neighbor approximation holds well in the range relevant for the extension of the H one-body density matrix, i.e., ± 1 Å. Dealing with the "kinematic uncorrelation" between the H nucleus and the other two nuclei, we have computed, through Eqs. (39) and (40), the following distribution $C(\mathbf{p}_H)$, a physical quantity

introduced in Eq. (20). Once the calculation was operated following exactly its definition (correlated),

$$
C(\mathbf{p}_H) = \int d\mathbf{p}_{F1} \int d\mathbf{p}_{F2} \, \mathbf{p}_{F2}^2 n_0(\mathbf{p}_{F1}, \mathbf{p}_H, \mathbf{p}_{F2}),
\tag{43}
$$

and later by assuming the aforementioned kinematic uncorrelation,
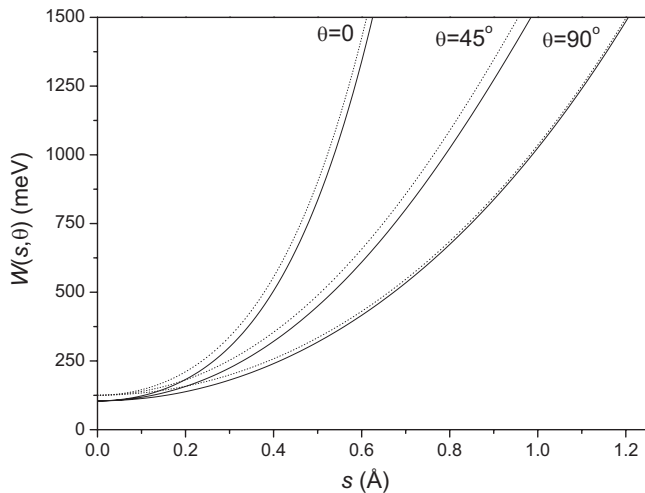
FIG. 6. Calculation of the effective potential $W(\mathbf{s})$ (see main text for its definition) felt by a H nucleus in an $[FHF]^-$ ion, as a function of $|\mathbf{s}|$ and for selected values of the azimuthal angle θ. Full lines represent the exact calculations, while dotted lines stand for evaluations making use of the adiabatic approximation for the fluorine ions.

$$C(\mathbf{p}_H) \simeq 2M_F\hbar^{-2}\langle E_k\rangle_F n_0^{(H)}(\mathbf{p}_H), \qquad (44)$$

where $\langle E_k\rangle_F$ is the fluorine-nucleus mean kinetic energy. Numerical results are reported in Fig. 7 as function of $|\mathbf{p}_H|$ for two values of θ: one ($\theta=0$) parallel to the molecular axis and the other ($\theta=90°$) perpendicular to it. It is clear from this figure that in our system, the mentioned kinematic uncorrelation between the H nucleus and the two F nuclei holds very precisely, casting no doubts on the theoretical possibility to reconstruct the potential felt by the H ion from its momentum distribution.
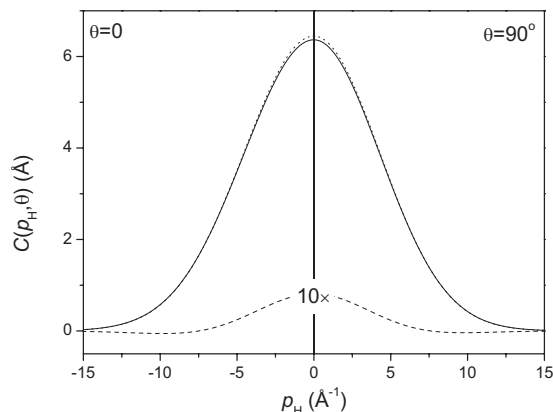
FIG. 7. Calculation of the distribution $C(\mathbf{p}_H)$ (see main text for its definition) shown by a H nucleus in an $[FHF]^-$ ion, as a function of $|\mathbf{p}_H|$ and for selected values of the azimuthal angle θ. Full lines represent the exact calculations, while dotted lines stand for evaluations making use of the uncorrelated approximation for F nuclei. The difference between the two calculations has also been plotted as a dashed line after a ten times magnification.
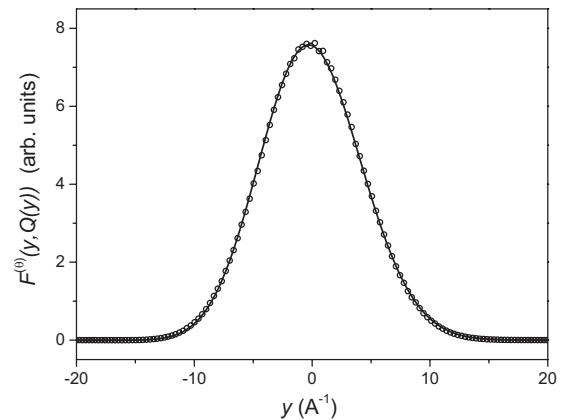
FIG. 8. Test of the convolution approximation used on VESU-VIO for a detector placed at a scattering angle $\theta=50.73°$. Circles represent $F_{sim}^{(\theta)}(y,Q(y))$, i.e., simulated data using an exact expression via a Monte Carlo code, while full line stands for $R_{sim}^{(\theta)}(y) \otimes F(y,Q(y))$, a calculated spectrum obtained through the convolution of a modified-Voigt resolution function times the NaHF$_2$ response function.

C. Test of the convolution approximation of the resolution function

The last aspect of the present discussion to be dealt with concerns the treatment of the VESUVIO spectrometer resolution known as "convolution approximation," already introduced in Sec. IV. Here, we would like to provide a full validation of the experimental procedure used to estimate the set of resolution functions $R^{(\theta)}(y)$ expressed as a modified Voigt distribution with θ-dependent parameters.[46] As mentioned above, an ancillary measurement on ZrH$_2$ has been operated on VESUVIO at room temperature. The choice of this compound was not casual, since it exhibits some peculiarities which make it the ideal VESUVIO calibrant for H scattering experiments: a well-known value of the proton mean kinetic energy [$\langle E_k\rangle_H=107.3$ meV (Ref. 63)], in addition to isotropic, harmonic, and almost undispersed H vibrations, even at room temperature. Under these conditions, the NCS response function $F(y,Q)$ is well described by Eq. (34), so that a fitting procedure of the experimental data can easily provide the best estimates of the resolution functions $R^{(\theta)}(y)$, which, convoluted with the response function [see Eq. (33)], are able to described the observed neutron spectra. The test consists in verifying how good these $R^{(\theta)}(y)$ are in describing the resolution effect in the case of scattering from protons in another compound, for example, NaHF$_2$, exhibiting a slightly different value of mean kinetic energy ($\langle E_k\rangle_H =111.8$ meV as in Sec. IV) and a more complex H dynamics. A number of NCS spectra $F_{sim}^{(\theta)}(y,Q(y))$ from ZrH$_2$ and NaHF$_2$ as measured on VESUVIO have been simulated through a dedicated Monte Carlo code,[64] which numerically implements Eq. (32), including FSE in the form of Eq. (34). One example, close to the middle of the detector angular range (namely, $\theta=50.73°$), is reported in Fig. 8. It is worth noting that this code employs the convolution approximation in no stage of its routines. Subsequently, simulated NCS

spectra from ZrH_2 were fitted through a convolution of modified Voigt distributions times the expression of Eq. (34), with $J(y)$ described by a Gaussian function ($\sigma=4.153$ Å^{-1}). In this way, a set of resolution functions for the simulated data, $R_{sim}^{(\theta)}(y)$, was determined. The last step of the present test consisted in folding these resolution functions with an appropriate $NaHF_2$ response function [still as in Eq. (34)] with $J(y)$ described by another Gaussian function ($\sigma=4.239$ Å^{-1}) and comparing the results, $R_{sim}^{(\theta)}(y) \otimes F(y,Q(y))$, to the simulated $F_{sim}^{(\theta)}(y,Q(y))$ for $NaHF_2$, where the convolution approximation was not applied. As clearly visible in Fig. 8, the agreement between the two sets of $NaHF_2$ spectra is excellent, proving that the extraction of the experimental $R^{(\theta)}(y)$ from the ancillary ZrH_2 measurements was a correct choice.

VII. CONCLUSIONS

In the present paper, neutron Compton scattering and incoherent inelastic neutron scattering measurements from polycrystalline sodium hydrogen fluoride at low temperature ($T<5$ K) have been presented and analyzed in order to study the proton dynamics in this strongly hydrogen-bonded system. Such an analysis has been performed in three distinct phases: (a) we set up a simple model for the short-time $NaHF_2$ response function, including deviations from the impulsive approximation due to neighbor atoms, which enabled the extraction of the proton mean kinetic energy through a fit of the experimental neutron Compton scattering data; (b) this estimate of the H mean kinetic energy was compared to an analogous result obtained from the hydrogen-projected density of phonon states, calculated through an *ab initio* lattice dynamics simulation making use of a well-assessed density functional theory code; and (c) finally the spectrum obtained from the vibrational neutron scattering measurements was used to validate the aforementioned simulation results, which turned out to be in excellent agreement with this spectrum. Unfortunately, the polycrystalline character of the sample, in conjunction with the limited statistical accuracy affecting the present neutron Compton scattering data, hindered a deeper data analysis, which, at least in principle, could shed light on further important aspects of the short-time H dynamics in $NaHF_2$, such as the H recoil peak shape, the final state effects, and the potential felt by the proton in this ionic compound. However, these aspects were studied in detail from the theoretical point of view, clarifying three important issues connected, more or less directly, to the H potential reconstruction: (1) the validity of the usual approach (essentially due to Sears[27]) to corrected for the final state effects in comparison with a more rigorous (and complex) procedure devised by Gersch *et al.*;[26] (2) the possibility to apply a one-body Schrödinger-like equation to the H momentum distribution in order to extract the proton potential surface (actually this problem was divided into two subproblems,

namely, the validity of the adiabatic approximation for the fluorine nuclei in an $[FHF]^-$ ion and the extent of the kinematic correlation between the H and F vibrations); and (3) the applicability of the so-called convolution approximation to include the instrumental resolution effects in the model response function used to analyze the NCS experimental data.

The results obtained for the $[FHF]^-$ ion in the study of the three aforementioned points were all substantially positive, proving that the proton potential surface is, in principle, derivable from neutron Compton scattering data on a $NaHF_2$ single-crystal exhibiting good statistical accuracy and narrow instrumental resolution. In detail, we have shown that in our system, the two procedures to calculate final state effects provide similar results (at least up to the $1/Q$ order), even taking into account the large anharmonic effects in the ion vibrational dynamics. Then, it has been proven that both requisites (i.e., the frozen neighbor and the uncorrelated kinematic approximations) needed for the potential extraction from the momentum distribution are satisfied. Finally, the convolution approximation for the treatment of the instrumental resolution effects is totally justified if the ancillary measurements are operated on ZrH_2, whose H mean kinetic energy does not excessively differ from the $NaHF_2$ one. As a possible future perspective for the topics of the present paper, a suitable subject could be represented by the proton dynamics in KH_2PO_4, where NCS data[19] reveal a double-well potential which is not found by accurate *ab initio* density functional theory simulations, at least keeping the heavier nuclei (K, P, and O) fixed in their equilibrium positions.[65,66] In this case, the situation might be different from that presented here for an isolated $[FHF]^-$ ion, where both assumptions required to move from a many-particle picture to a single-proton one (namely kinematic uncorrelation and frozen neighbor approximation) appear to hold satisfactorily. Given the theoretical importance of KH_2PO_4 (being a classic paradigm for ferroelectricity), simulation study on this compound making use of the conceptual tools we have introduced here would be surely of relevant interest, especially to understand what NCS can actually probe in KH_2PO_4.

[1] C. Andreani, D. Colognesi, J. Mayers, G. F. Reiter, and R. Senesi, Adv. Phys. **54**, 377 (2005).

[2] V. I. Gol'danskiĭ, Sov. Phys. JETP **4**, 604 (1957).

[3] M. Bée, *Quasielastic Neutron Scattering* (Hilger, Bristol, 1988).

[4] P. C. H. Mitchell, S. F. Parker, A. J. Ramirez-Cuesta, and J. Tomkinson, *Vibrational Spectroscopy with Neutrons with Applications in Chemistry, Biology, Materials Science and Catalysis* (World Scientific, Singapore, 2005).

[5] C. A. Chatzidimitriou-Dreismann, T. A. Redah, R. M. F. Streffer, and J. Mayers, Phys. Rev. Lett. **79**, 2839 (1997); E. B. Karlsson, C. A. Chatzidimitriou-Dreismann, T. Abdul-Redah, R. M. F. Streffer, B. Hjörvarsson, J. Öhrmalm, and J. Mayers, Europhys. Lett. **46**, 617 (1999).

[6] D. Colognesi, Physica B **344**, 73 (2004); **358**, 114 (2005).

[7] R. Senesi, D. Colognesi, A. Pietropaolo, and T. Abdul-Redah, Phys. Rev. B **72**, 054119 (2005); R. A. Cowley and J. Mayers, J. Phys.: Condens. Matter **18**, 5291 (2006), and references therein.

[8] C. A. Chatzidimitriou-Dreismann, Acta Phys. Hung. B **26**, 203 (2006).

[9] W. Hayes and R. Loudon, *Scattering of Light by Crystals* (Dover, Minneola, NY, 2004); D. Porezag and M. R. Pederson, Phys. Rev. B **54**, 7830 (1996).

[10] G. S. Samosvat, Yu. S. Sayasov, and V. T. Chuburkov, Sov. Phys. JETP **27**, 15 (1968).

[11] R. M. Brugger, A. D. Taylor, C. E. Olsen, J. A. Goldstone, and A. K. Soper, Nucl. Instrum. Methods Phys. Res. A **221**, 393 (1984); A. K. Soper and A. D. Taylor, Los Alamos Report No. LA-10227, 1984 (unpublished), Vol. II, p. 611.

[12] A. C. Evans, J. Mayers, D. N. Timms, and M. J. Cooper, Z. Naturforsch., A: Phys. Sci. **48**, 425 (1993).

[13] J. Mayers, J. Tomkinson, T. Abdul-Redah, W. G. Stirling, C. Andreani, R. Senesi, M. Nardone, D. Colognesi, and E. Degiorgi, Physica B **350**, E659 (2004).

[14] See H. R. Glyde, *Excitations in Liquid and Solid Helium* (Oxford University Press, Oxford, 1994), and references therein.

[15] J. Mayers, Phys. Rev. Lett. **71**, 1553 (1993); C. Andreani, A. Filabozzi, and E. Pace, Phys. Rev. B **51**, 8854 (1995); M. P. Zinkin, R. A. Cowley, R. S. Eccleston, A. C. Evans, and M. J. Harris, Can. J. Phys. **73**, 772 (1995).

[16] G. K. Ivanov and Yu. S. Sayasov, Usp. Fiz. Nauk **90**, 47 (1966); G. K. Ivanov and Yu. S. Sayasov, Sov. Phys. Usp. **9**, 670 (1967).

[17] D. Colognesi and E. Pace, Physica B **266**, 267 (1999); D. Colognesi, E. Degiorgi, and E. Pace, *ibid.* **293**, 317 (2001).

[18] C. Andreani, E. Degiorgi, R. Senesi, F. Cilloco, D. Colognesi, J. Mayers, M. Nardone, and E. Pace, J. Chem. Phys. **114**, 387 (2001).

[19] G. F. Reiter, J. Mayers, and P. Platzman, Phys. Rev. Lett. **89**, 135505 (2002).

[20] E. B. Karlsson and S. W. Lovesey, Phys. Rev. A **61**, 062714 (2000).

[21] N. I. Gidopoulos, Phys. Rev. B **71**, 054106 (2005); G. F. Reiter and P. M. Platzman, *ibid.* **71**, 054107 (2005).

[22] G. I. Watson, J. Phys.: Condens. Matter **8**, 5955 (1996).

[23] G. F. Chew, Phys. Rev. **80**, 196 (1950).

[24] S. W. Lovesey, *Theory of Neutron Scattering from Condensed Matter* (Clarendon, Oxford, 1984).

[25] J. M. F. Gunn, C. Andreani, and J. Mayers, J. Phys. C **19**, L835 (1986); J. J. Weinstein and J. W. Negele, Phys. Rev. Lett. **49**, 1016 (1982); E. Pace, G. Salmè, and G. B. West, Phys. Lett. B **273**, 205 (1991).

[26] H. A. Gersch, L. J. Rodriguez, and P. N. Smith, Phys. Rev. A **5**, 1547 (1972); H. A. Gersch and L. J. Rodriguez, Phys. Rev. A **8**, 905 (1973).

[27] V. F. Sears, Phys. Rev. B **30**, 44 (1984).

[28] A. S. Rinat and M. F. Taragin, Phys. Rev. B **41**, 4247 (1990).

[29] A. S. Rinat and M. F. Taragin, Phys. Rev. B **58**, 15011 (1998).

[30] A. S. Rinat, M. F. Taragin, F. Mazzanti, and A. Polls, Phys. Rev. B **57**, 5347 (1998).

[31] Yejun Feng, C. Ancona-Torres, T. F. Rosenbaum, G. F. Reiter, D. L. Price, and E. Courtens, Phys. Rev. Lett. **97**, 145501 (2006).

[32] G. F. Reiter, J. Mayers, and J. Noreland, Phys. Rev. B **65**, 104305 (2002).

[33] G. Reiter, J. C. Li, J. Mayers, T. Abdul-Redah, and P. Platzman, Braz. J. Phys. **34**, 142 (2004); C. J. Burnham, G. F. Reiter, J. Mayers, T. Abdul-Redah, H. Reichert, and H. Dosch, Phys. Chem. Chem. Phys. **8**, 3966 (2006).

[34] G. Reiter, C. Burnham, D. Homouz, P. M. Platzman, J. Mayers, T. Abdul-Redah, A. P. Moravsky, J. C. Li, C.-K. Loong, and A. I. Kolesnikov, Phys. Rev. Lett. **97**, 247801 (2006).

[35] G. F. Reiter, J. Mayers, and T. Abdul-Redah, Physica B **385-386**, 234 (2006).

[36] A. Guinier, *X-ray Diffraction in Crystals, Imperfect Crystals and Amorphous Bodies* (Dover, Mineola, NY, 1994).

[37] G. A. Jeffrey, *An Introduction to Hydrogen Bonding* (Oxford University Press, Oxford, 1997).

[38] P. Dawson, M. M. Hargreave, and G. R. Wilkinson, Spectrochim. Acta, Part A **31**, 1055 (1975).

[39] T. B. McMahon and J. W. Larson, J. Am. Chem. Soc. **104**, 5848 (1982).

[40] J. J. Rush, L. W. Schroeder, and A. J. Melveger, J. Chem. Phys. **36**, 2793 (1972).

[41] R. D. Cooke, C. Pastorek, R. E. Carlson, and J. C. Decius, J. Chem. Phys. **69**, 5 (1978).

[42] H. Boutin, G. J. Safford, and V. Brajovic, J. Chem. Phys. **36**, 2793 (1972).

[43] G. K. Kearley, J. Tomkinson, and J. Penfold, Z. Phys. B: Condens. Matter **69**, 63 (1987).

[44] R. W. Wyckoff, *Crystal Structures* (Interscience, New York, 1972), Vol. II.

[45] A. G. Christy, J. Haines, and S. M. Clark, J. Phys.: Condens. Matter **4**, 8131 (1992).

[46] E. M. Schooneveld, J. Mayers, N. J. Rhodes, A. Pietropaolo, C. Andreani, R. Senesi, G. Gorini, E. Perelli-Cippo, and M. Tardocchi, Rev. Sci. Instrum. **77**, 095103 (2006).

[47] D. Colognesi, M. Celli, F. Cilloco, R. J. Newport, S. F. Parker, V. Rossi-Albertini, F. Sacchetti, J. Tomkinson, and M. Zoppi, Appl. Phys. A: Mater. Sci. Process. **74**, s64 (2002).

[48] J. Mayers and A. C. Evans, RAL Technical Report No. RAL-TR-96-044, 1996 (unpublished); J. Mayers, RAL Technical Report No. RAL-TR-96-067, 1996 (unpublished).

[49] J. Mayers and T. Abdul-Redah, J. Phys.: Condens. Matter **16**, 4811 (2004); J. J. Blostein, J. Dawidowski, and J. R. Granada, Phys. Rev. B **71**, 054105 (2005), and references therein.

[50] S. F. Parker, J. Tomkinson, A. J. Ramirez-Cuesta, and D. Colognesi, RAL Technical Report No. RAL-TR-2003-015, 2003 (unpublished).

[51] A. K. Agrawal, Phys. Rev. A **4**, 1560 (1971); V. F. Sears, Adv. Phys. **24**, 1 (1975).

[52] D. Colognesi, C. Andreani, and E. Degiorgi, J. Neutron Res. **11**,

123 (2003).

[53] X. Gonze, J.-M. Beuken, R. Caracas, F. Detraux, M. Fuchs, G.-M. Rignanese, L. Sindic, M. Verstraete, G. Zerah, F. Jollet, M. Torrent, A. Roy, M. Mikami, Ph. Ghosez, J.-Y. Raty, and D. C. Allan, Comput. Mater. Sci. **25**, 478 (2002).

[54] C. Hartwigsen, S. Goedecker, and J. Hutter, Phys. Rev. B **58**, 3641 (1998).

[55] J. P. Perdew, K. Burke, and M. Ernzerhof, Phys. Rev. Lett. **77**, 3865 (1996).

[56] G. D. Barrera, D. Colognesi, P. C. H. Mitchell, and A. J. Ramirez-Cuesta, Chem. Phys. **317**, 119 (2005).

[57] K. Refson, P. R. Tulip, and S. J. Clark, Phys. Rev. B **73**, 155114 (2006).

[58] X. Gonze and C. Lee, Phys. Rev. B **55**, 10355 (1997).

[59] A. J. Ramirez-Cuesta, Comput. Phys. Commun. **157**, 226 (2004).

[60] J. Penfold and J. Tomkinson, RAL Technical Report No. RAL-86-019, 1986 (unpublished).

[61] B. L. McGaw and J. A. Ibers, J. Chem. Phys. **39**, 2677 (1963).

[62] L. L. Lohr, Jr. and R. J. Sloboda, J. Phys. Chem. **85**, 1332 (1981).

[63] A. C. Evans, D. N. Timms, J. Mayers, and S. M. Bennington, Phys. Rev. B **53**, 3023 (1996).

[64] J. Mayers, A. L. Fielding, and R. Senesi, Nucl. Instrum. Methods Phys. Res. A **481**, 454 (2002).

[65] S. Koval, J. Kohanoff, R. L. Migoni, and E. Tosatti, Phys. Rev. Lett. **89**, 187602 (2002).

[66] S. Koval, J. Kohanoff, J. Lasave, G. Colizzi, and R. L. Migoni, Phys. Rev. B **71**, 184102 (2005).